Migration of Ground Penetrating Radar With Antenna Radiation Pattern Correction

Hai Liu, *Senior Member, IEEE*, Zhijie Chen, Hantao Lu, Feng Han, *Senior Member, IEEE*, Chao Liu, Jing Li, and Jie Cui

***Abstract*— Migration can reconstruct the geometric structure of a subsurface object from the ground penetrating radar (GPR) data. However, a GPR antenna is usually simplified as an ideal point/line source of normal migration algorithms, which ignore the influence of the antenna radiation pattern in subsurface soil. In this letter, the back-propagation algorithm is corrected with the analytical half-space far-field radiation pattern of an infinite line source. The superiority of this modified migration algorithm is verified through numerical, laboratory, and field experiments. The results show that the undesired diffractive artifacts at the target edges can be suppressed, while reserving the reflection amplitude in the migrated images with antenna pattern correction, compared with the conventional back-propagation and Kirchhoff algorithms.**

***Index Terms*— Antenna radiation pattern, back-propagation, ground penetrating radar (GPR), Kirchhoff migration, migration.**

I. Introduction

GROUND PENETRATING radar (GPR), as a recognized geophysical method utilizing high-frequency electromagnetic (EM) waves [1], has been widely applied in various fields, such as civil engineering [2], landmine and utility detection [3], [4], and space exploration [5]. Due to the wide beamwidth of a GPR antenna and the target scattering, the recorded raw GPR profile is far from the actual geometry of a complicated subsurface structure. Migration, which is initially used for seismic data processing, can move oblique layers to their true subsurface positions, collapse the diffraction, and enhance the spatial resolution [6] and, thus, becomes a common GPR processing tool.

Various migration algorithms, such as diffraction stack [7], Kirchhoff migration [8], back propagation [9], phase shift migration [10], Stolt migration [11], and reverse time migration (RTM) [12], have been applied to GPR data processing. Recent advances in GPR migration algorithms have increased its ability to image complex subsurface structures. An autofocusing technique based on a generalized multilayer Stolt migration was proposed to estimate geometries of subsurface oblique layers [13]. Zhuge *et al.* [14] modified the Kirchhoff migration algorithm for multiinput multioutput array-based radar imaging in both the free space and underground space. Liu *et al.* [15] proposed a frequency-domain RTM algorithm based on layered medium Green's functions, which greatly reduces the computational cost by a magnitude of two orders. Feng *et al.* [16] presented a polarimetric migration method for GPR imaging, which is able to classify the geometries of subsurface targets. Zhu *et al.* [17] modified the RTM algorithm to compensate the GPR data attenuation. In these scalar migration algorithms, GPR antennas are simplified as an ideal point source in 3-D cases or a line source in 2-D cases, from which EM waves are radiated equally in all directions. However, the radiation pattern of a dipole or a real GPR antenna lying horizontally on the interface of a half-space is far from that of an omnidirectional antenna in free space [18].

For an infinitesimal dipole and an infinite line source horizontally lying on the interface of a half-space, their far-field radiation patterns in subsurface can be calculated by an analytic solution [18], [19]. For a realistic GPR antenna, its radiation pattern can be obtained by numerical modeling [20] or a well-designed laboratory experiment [21], [22]. The accuracy of imaging reconstruction by microwave tomography has been verified to be improved through taking into account of the simulated GPR antenna pattern [20]. A vector phase shift migration algorithm that accounts for the radiation characteristics of a dipole antenna through calculating the Green's functions has been proposed and can improve the imaging quality of dipping layers [23], [24]. However, the evaluation of the Green's functions is computationally expensive. The far-field radiation pattern of a horizontal dipole [18] is explicitly incorporated into the Kirchhoff migration algorithm [8], but its effect requires further discussion.

In this letter, the influence of antenna radiation pattern on migrated images is investigated. Specifically, the back-propagation algorithm is corrected by incorporating the half-space far-field radiation pattern of an infinite line source [19], and the benefit is validated through numerical, laboratory, and field experiments. The rest of this letter is organized as follows. The migration algorithm with antenna radiation pattern correction is introduced in Section II. Section III presents the experimental results and is followed by the conclusions in Section IV.

II. Methods

We use a modified back-propagation algorithm, which is integrated with a simple correction factor of the half-space far-field antenna radiation pattern in subsurface, to investigate its effect on the migration results. The modified algorithm,

Manuscript received March 6, 2020; revised July 18, 2020; accepted September 18, 2020. Date of publication October 6, 2020; date of current version December 17, 2021. This work was supported in part by the National Key Research and Development Program of China under Grant 2017YFC1500400 and Grant 2016YFC0802400; in part by the National Natural Science Foundation of China under Grant 41874120, Grant 41874134, and Grant 51778159; and in part by the Research Program of Bureau of Education of Guangzhou, China under Grant 201831804. *(Corresponding authors: Chao Liu; Jing Li.)*

Hai Liu, Zhijie Chen, Chao Liu, and Jie Cui are with the School of Civil Engineering, Guangzhou University, Guangzhou 510006, China (e-mail: hliu@gzhu.edu.cn; chaoliu@gzhu.edu.cn; jcui@gzhu.edu.cn).

Hantao Lu and Feng Han are with the Key Laboratory of Electromagnetic Wave Science and Detection Technology, Institute of Electromagnetics and Acoustics, Xiamen University, Xiamen 361005, China (e-mail: feng.han@xmu.edu.cn).

Jing Li is with the College of Geo-Exploration Science and Technology, Jilin University, Changchun 130026, China (e-mail: jwy1209@163.com).

Digital Object Identifier 10.1109/LGRS.2020.3026207

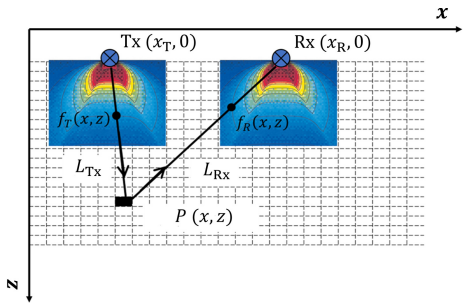

Fig. 1. Schematic of the back-propagation algorithm with antenna radiation pattern correction.

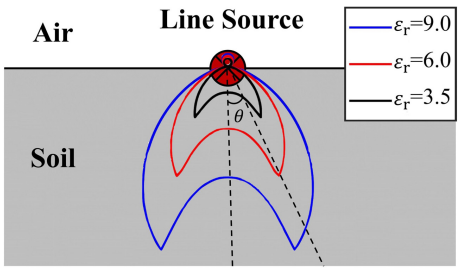

Fig. 2. Radiation patterns of an infinite line source lying on a homogeneous air–soil model, of which the relative dielectric permittivity of soil is 3.5, 6.0, and 9.0.

as well as the Kirchhoff migration algorithm, is introduced in this section.

A. Migration With Antenna Pattern Correction

A schematic illustration of back-propagation algorithm with antenna radiation pattern correction is shown in Fig. 1. A bistatic measurement mode is considered, and the transmitter and receiver lay on the interface of a homogeneous half-space. Thus, the two-way travel time of the reflected signal from the transmitter to an arbitrary imaging point in subsurface and back to the receiver is given by

$$t(x,z) = \frac{L_{\mathrm{Tx}} + L_{\mathrm{Rx}}}{v} = \frac{\sqrt{(x_{\mathrm{T}}-x)^2+z^2} + \sqrt{(x_{\mathrm{R}}-x)^2+z^2}}{v} \tag{1}$$

where v is the propagation velocity of GPR waves in the subsurface medium, L_{Tx} and L_{Rx} are the downward and upward paths of reflected signal from the imaging point $P(x, z)$, respectively, and x_{T} and x_{R} are the horizontal coordinates of the transmitter and receiver, respectively.

When a common-offset GPR antenna moves along a survey line on the ground surface, the travel time–distance trajectory of a point reflection is approximately a hyperbolic curve. A conventional back-propagation algorithm assumes that the source radiates energy equally in all directions and focuses the image by stacking the energy along the hyperbolic trajectory using the following equation:

$$S(x,y) = \sum_{i=1}^{n} E_i(t_i(x,z)) \tag{2}$$

where $E_i(t_i)$ is the amplitude of GPR signal recorded at the ith station (antenna position) at the two-way travel time t_i, which is given by (1).

The modified migration algorithm considers a normalized antenna radiation pattern as a weight coefficient. As illustrated in Fig. 1, the view angles of each imaging point relative to the transmitter and receiver are known and the corresponding weight coefficients can be obtained from the radiation pattern. Thus, the back-propagation algorithm with an antenna pattern correction is given by

$$S_{\mathrm{APC}}(x,y) = \sum_{i=1}^{n} f_{\mathrm{R},i} \cdot f_{\mathrm{T},i} \cdot E_i(t_i(x,z)) \tag{3}$$

where $f_{\mathrm{T},i}$ and $f_{\mathrm{R},i}$ are the correction factors corresponding the radiation patterns of the transmitter and receiver, respectively. When the GPR antenna is at the ith station, the correction factors can be obtained from a known radiation pattern according to the angles between the ray paths and the vertical direction illustrated in Fig. 1. The method to obtain the antenna radiation pattern is introduced in Section II-B.

B. Antenna Radiation Pattern

As mentioned above, the radiation pattern of a GPR antenna can be modeled by a full-wave simulation or measured in laboratory. However, we know that the GPR antennas usually operate in the proximity of the ground surface. Thus, the antenna radiation pattern is strongly affected by the dielectric properties of the subsurface soil, which greatly changes in different environments. The simulation or measurement of GPR antenna radiation patterns in different conditions would be time consuming and labor consuming. Without losing generality, the analytical solution of the half-space far-field radiation pattern of an infinite line source is used to calculate the pattern correction factors in (3), and its expression is given by [19]

$$f(\theta) = \begin{cases} A \cdot \left(n\cos^2\theta - \cos\theta \cdot \sqrt{1-n^2\sin^2\theta}\right)^2 \\ (-\theta_c \le \theta \le \theta_c) \\ A \cdot \left(n^2\cos^4\theta + \cos^2\theta \cdot \sqrt{n^2\sin^2\theta - 1}\right) \\ \left(-\dfrac{\pi}{2} \le \theta \le \theta_c, \theta_c \le \theta \le \dfrac{\pi}{2}\right) \end{cases} \tag{4}$$

where $A = (\omega\mu_0 I^2/4\pi\rho)(n^2/(n^2-1)^2)$, ω is the angular frequency, I is the exciting current, $n = \sqrt{(\varepsilon_0/\varepsilon)}$ is the refractive index, $\theta_c = \sin^{-1}(1/n)$ is the critical angle, θ is the angle between the propagation direction and the vertical axis, and ε is the dielectric permittivity of the subsurface soil. It is noteworthy that the analytical solution is frequency invariant.

Fig. 2 shows the H-field radiation patterns of an infinite line source calculated by (4), when the relative permittivity of the subsurface soil is 3, 6, and 9. We can see that most energy is radiated into the subsurface soil and the ratio increases with the soil permittivity. The pattern in subsurface has two lobes, and the maximum radiation direction corresponds to the critical angle [19].

C. Kirchhoff Migration

In order to validate the effectiveness of modified back-propagation algorithm with antenna radiation pattern correction, we also briefly introduce the Kirchhoff migration as a reference. The formulation of 2-D Kirchhoff migration can be expressed by [25]

$$P(x,z) = \frac{1}{2\pi}\sum_{i=1}^{n} \frac{\cos\theta}{\sqrt{vR}} \frac{\partial}{\partial t} E_i(t_i(x,z)) \tag{5}$$

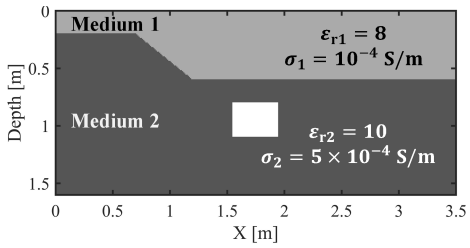

Fig. 3. Simulation model in the numerical experiment.

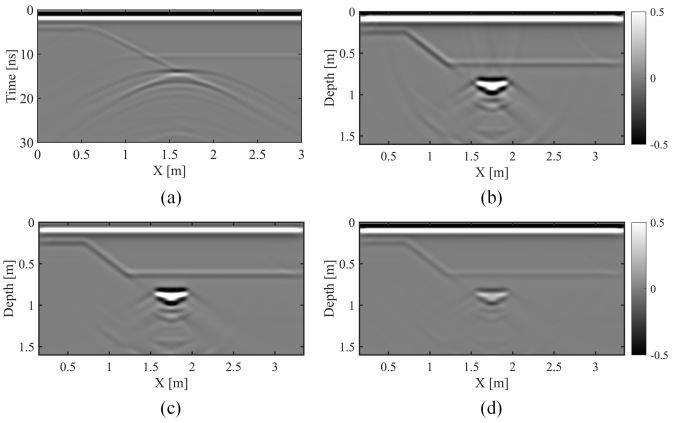

Fig. 4. Numerical experiment results. (a) Simulated raw GPR B-scan profile and migrated images by (b) conventional back propagation, (c) modified back propagation with antenna radiation pattern correction, and (d) Kirchhoff migration.

where $R = L_{\mathrm{Tx}} + L_{\mathrm{Rx}}$ is the two-way travel path. The inclination factor $\cos\theta$ approximates the amplitude change with the radiation direction [3]. Therefore, Kirchhoff migration can be considered to have integrated a simple correction of the antenna pattern, of which the maximum amplitude is in the vertically downward direction [8]. Note that the half time derivation will introduce a 45° phase shift in the 2-D Kirchhoff migration. However, we omit the time derivation for a fair comparison with the back-propagation migration.

III. Experiments and Results

In this section, we present the results of a numerical experiment, a laboratory experiment, and a field experiment to verify the performance of the proposed modified migration with antenna radiation pattern correction, compared with the conventional back-propagation algorithm and the Kirchhoff migration.

A. Numerical Experiment

As shown in Fig. 3, the 2-D simulation model consists of two media with a stair-stepping interface and an air void buried in Medium 2. The GPR antenna on the ground surface is simulated as an infinite line source, of which the polarization is in the y-direction. The radiation pattern of the line source in the first subsurface layer (Medium 1) is accurately depicted in Fig. 2 by (4). The source excitation is a Ricker wavelet with a central frequency of 400 MHz. A common-offset GPR data set is simulated by the finite-difference time-domain (FDTD) method. As shown in Fig. 4(a), two strong hyperbolic reflections from the top and bottom of the air void can

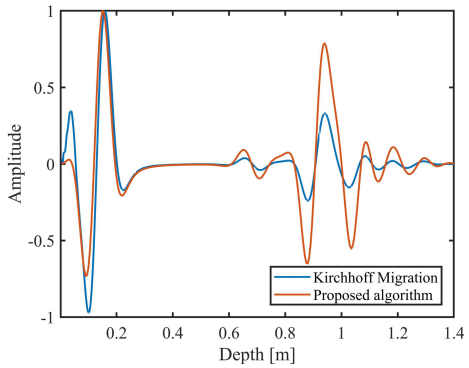

Fig. 5. Comparison between the GPR traces over the simulated air void migrated by Kirchhoff migration and the proposed algorithm.

be observed. However, the actual geometry of the subsurface structure can be hardly interpreted from the raw GPR profile.

The GPR images migrated using a homogeneous velocity model are shown in Fig. 4(b)–(d). In the reconstructed image by the conventional back-propagation algorithm in Fig. 4(b), the inclined interface has been moved to its actual position and the top of the rectangular air void is well focused. The bottom of the void is over migrated to be a "smile," because the velocity in Medium 1 is used for migration, which is different from those in air and Medium 2. However, we can still see strong diffractive artifacts at the top corners and of the void. In contrast, these diffractive artifacts have been well suppressed in the migrated image by the modified back-propagation algorithm with antenna pattern correction in Fig. 4(c). The reconstructed image in Fig. 4(d) shows that Kirchhoff migration can also suppress the diffractive artifacts at the corners but reduces the intensity of the target reflection, compared with Fig. 4(c). Comparison between the GPR traces over the simulated air void further demonstrates that Kirchhoff migration results in a smaller reflection amplitude, compared with the proposed algorithm, as shown in Fig. 5. Therefore, inclusion of an accurate correction of the antenna pattern in the back-propagation algorithm can improve the migration accuracy, while preserving the amplitude information.

A contrast metric is introduced to quantitatively evaluate the imaging quality of reconstructed images. It is expressed by [26]

$$C = \frac{\sqrt{\sum_{i=1}^{m}\sum_{j=1}^{n}\left\{\left|u(x_i,z_j)\right|^2 - \alpha(x_i,z_j)\right\}^2}}{\sum_{i=1}^{m}\sum_{j=1}^{n}\left|u(x_i,z_j)\right|^4} \tag{6}$$

where m and n represent the pixel number of rows and columns in the migrated image, $u(x_i, z_j)$ is the amplitude of the pixel, and $\alpha(x_i, z_j)$ is given by

$$\alpha(x_i,z_j) = \frac{\sum_{i}^{m}\sum_{j}^{n}\left|u(x_i,z_j)\right|^4}{mn}. \tag{7}$$

The migrated image corresponding to larger value of contrast metric is considered to have a better migration performance. The contrast metric of Fig. 4(b)–(d) is 1.10, 1.18, and 0.99, respectively. It means that the antenna pattern correction improves the imaging quality.

B. Laboratory Experiment

A laboratory experiment was carried out to further verify the effectiveness of the antenna pattern correction for migration

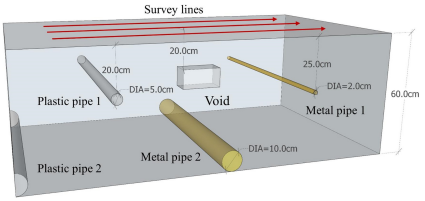

Fig. 6. Setup of the laboratory experiment.

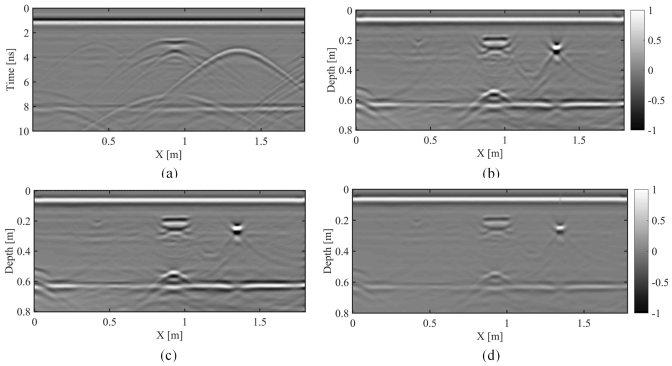

Fig. 7. Laboratory experiment results. (a) Recorded GPR raw B-scan profile and migrated images by (b) conventional back propagation, (c) modified back propagation with antenna radiation pattern correction, and (d) Kirchhoff migration.

when it is applied to GPR data measured by a real antenna. The experiment was conducted on a sandpit, which has a depth of 60 cm. The relative permittivity of the dry sand is about 3.5. Two plastic pipes, an air void, and two metal pipes were buried in the sand, as shown in Fig. 6. The rectangular air-filled void is made of glass with a dimension of 20 cm $\times$ 10 cm $\times$ 10 cm. GPR data were recorded using a commercial GPR system with a 2-GHz bowtie antenna. Parallel GPR survey lines were set on a plastic plate to avoid the spin of the distance-measuring wheel equipped on the antenna on the sand surface and to ensure that the antenna move along a straight line. Gridded 3-D GPR data were acquired on a survey area of 175 cm $\times$ 110 cm with 55 survey lines.

The raw GPR profile collected on the survey line over the middle of the air void is shown in Fig. 7(a). The hyperbolic reflection from the buried pipes and the horizontal reflection from the bottom of the sandpit can be clearly identified. For the air void, two intersecting hyperbolic reflections from the two edges of its top surface and a hyperbolic reflection from its bottom surface can be observed. Nevertheless, the shape of the air void can hardly be identified. The GPR images migrated using a homogeneous velocity model ($v = 0.162$ m/ns) are shown in Fig. 7(b)–(d). In the reconstructed image by the conventional back-propagation algorithm in Fig. 7(b), the rectangular shape of the air void is well presented. However, undesired diffractive artifacts form the corners of the air void show up. The diffractive artifacts from the focused spot of the metal pipe on the right are also observed. In contrast, these diffractive artifacts have been suppressed to a certain extent in the migrated image by the modified back-propagation algorithm with the antenna radiation pattern correction in Fig. 7(c). Compared with Fig. 7(c), the reconstructed image in Fig. 7(d) shows that Kirchhoff migration can also suppress the diffractive artifacts at the corners but reduces the reflection intensity of the target reflection. The comparison between GPR traces

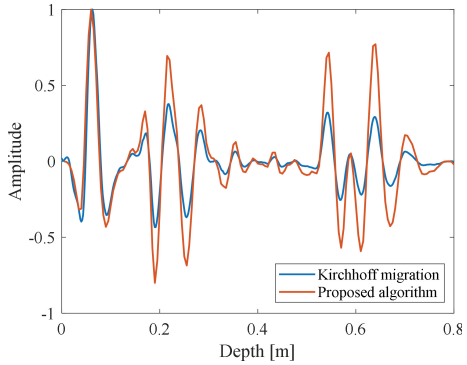

Fig. 8. Comparison between the GPR traces over the air void migrated by Kirchhoff migration and the proposed algorithm.

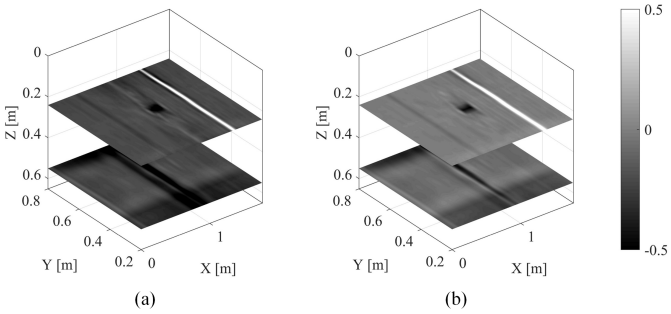

Fig. 9. Horizontal slices reconstructed by back-propagation migration (a) without and (b) with the antenna radiation pattern correction.

over the air void in Fig. 8 further verifies that the proposed algorithm can obtain stronger reflection energy compared with Kirchhoff migration. Contrast metric of Fig. 7(b)–(d) is 1.45, 1.51, and 1.33, respectively. Hence, we can conclude that the imaging accuracy can be improved after the antenna radiation pattern correction.

Through reconstructing all the 55 GPR profiles by 2-D migration, a 3-D cube of migrated GPR data is obtained. Two horizontal slices at different depths are shown in Fig. 9. At the shallow depth, the geometric shapes of tin two pipes and the air cavity can be clearly discriminated. It should be noted that the air cavity is better focused with an improved contrast in the migrated image with antenna radiation pattern correction in Fig. 9(b), compared with that in Fig. 9(a). As a result, it is easier to interpret its shape and size. Therefore, it is concluded that the correction of the half-space far-field radiation pattern of an ideal infinite line source in subsurface is also effective for a real GPR antenna. The reason is that most GPR systems use resistively loaded dipole, bowtie, or horn antennas, which can be considered as a type of broadband dipole antenna and have a similar radiation pattern in subsurface with an infinite line source.

C. Field Experiment

The proposed method is further validated by a field experiment. A GPR profile was acquired using a commercial GPR system with a 400-MHz antenna over a buried plastic water pipe under a paved road on campus. The depth to the top of the pipe and its diameter are 50 and 30 cm, respectively. After data preprocessing including zero-time correction, bandpass filtering, background removal, and gain, the original GPR profile is shown in Fig. 10(a). A hyperbolic reflection from the

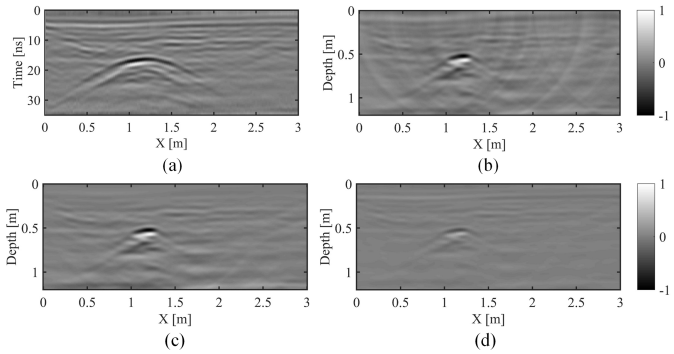

Fig. 10. Field experiment results. (a) Recorded GPR profile and migrated images by (b) conventional back propagation, (c) modified back propagation with antenna radiation pattern correction, and (d) Kirchhoff migration.

buried pipe can be clearly discerned, although strong clutters also exist.

The GPR images migrated using a homogeneous velocity model ($v = 0.068$ m/ns) are shown in Fig. 10(b)–(d). In the reconstructed image by the conventional back-propagation algorithm in Fig. 10(b), the top surface of the buried pipe is well focused. However, a number of upward-opening hyperbolic artifacts show up. After the antenna pattern correction, these artifacts are well suppressed in Fig. 10(c). The Kirchhoff migration can also suppress these artifacts but sacrifices the amplitude of the pipe reflection in Fig. 10(d). Contrast metric of Fig. 10(b)–(d) is 1.10, 1.26, and 1.15, respectively. Thus, we conclude that the proposed migration with antenna radiation pattern correction is effective in a GPR field experiment.

IV. Conclusion

In this letter, the influence of the antenna radiation pattern on GPR migration is investigated by integrating the subsurface pattern of an infinite line source lying on the ground surface into the back-propagation algorithm. Based on the numerical, laboratory, and field experimental results, it is concluded that the imaging accuracy can be improved by introducing the antenna radiation pattern correction and the correction using the line source pattern is effective for the real dipole-type GPR antenna. Compared with the Kirchhoff migration, the proposed migration method can preserve the amplitude information of target reflection.

References

[1] H. M. Jol, *Ground Penetrating Radar Theory and Applications*. Amsterdam, The Netherlands: Elsevier, 2009.

[2] H. Liu, C. Lin, J. Cui, L. Fan, X. Xie, and B. F. Spencer, "Detection and localization of rebar in concrete by deep learning using ground penetrating radar," *Autom. Construct.*, vol. 118, no. 10, pp. 1–12, 2020, doi: 10.1016/j.autcon.2020.103279.

[3] X. Feng and M. Sato, "Pre-stack migration applied to GPR for landmine detection," *Inverse Problem*, vol. 20, pp. S99–S115, Nov. 2004, doi: 10.1088/0266-5611/20/6/S07.

[4] H. Liu, X. Huang, F. Han, J. Cui, B. F. Spencer, and X. Xie, "Hybrid polarimetric GPR calibration and elongated object orientation estimation," *IEEE J. Sel. Topics Appl. Earth Observ. Remote Sens.*, vol. 12, no. 7, pp. 2080–2087, Jul. 2019, doi: 10.1109/JSTARS.2019.2912339.

[5] L. Xiao *et al.*, "A young multilayered terrane of the northern mare imbrium revealed by Chang'E-3 mission," *Science*, vol. 347, no. 6227, pp. 1226–1229, Mar. 2015, doi: 10.1126/science.1259866.

[6] C. Özdemir, Ş. Demirci, E. Yiğit, and B. Yilmaz, "A review on migration methods in B-scan ground penetrating radar imaging," *Math. Problems Eng.*, vol. 2014, pp. 1–16, Jun. 2014, doi: 10.1155/2014/280738.

[7] J. Schofield, D. Daniels, and P. Hammerton, "A multiple migration and stacking algorithm designed for land mine detection," *IEEE Trans. Geosci. Remote Sens.*, vol. 52, no. 11, pp. 6983–6988, Nov. 2014, doi: 10.1109/TGRS.2014.2306325.

[8] M. L. Moran, R. J. Greenfield, S. A. Arcone, and A. J. Delaney, "Multidimensional GPR array processing using Kirchhoff migration," *J. Appl. Geophys.*, vol. 43, nos. 2–4, pp. 281–295, Mar. 2000, doi: 10.1016/S0926-9851(99)00065-8.

[9] L. Zhou, C. Huang, and Y. Su, "A fast back-projection algorithm based on cross correlation for gpr imaging," *IEEE Geosci. Remote Sens. Lett.*, vol. 9, no. 2, pp. 228–232, Mar. 2012, doi: 10.1109/LGRS.2011.2165523.

[10] T. Olofsson, "Phase shift migration for imaging layered objects and objects immersed in water," *IEEE Trans. Ultrason., Ferroelectr., Freq. Control*, vol. 57, no. 11, pp. 2522–2530, Nov. 2010, doi: 10.1109/TUFFC.2010.1718.

[11] M. A. Gonzalez-Huici, "Adaptative Stolt migration via contrast maximization for GPR applications," in *Proc. 6th Int. Workshop Adv. Ground Penetrating Radar (IWAGPR)*, Jun. 2011, pp. 1–5, doi: 10.1109/IWAGPR.2011.5963855.

[12] H. Liu, Y. Qi, Z. Chen, H. Tong, C. Liu, and M. Zhuang, "Ultrasonic inspection of grouted splice sleeves in precast concrete structures using elastic reverse time migration method," *Mech. Syst. Signal Process.*, vol. 148, no. 107152, pp. 1–11, 2021, doi: 10.1016/j.ymssp.2020.

[13] H. Jung and K. Kim, "Autofocusing technique based on generalized multilayer stolt migration," *IEEE Trans. Geosci. Remote Sens.*, vol. 56, no. 3, pp. 1386–1393, Mar. 2018, doi: 10.1109/TGRS.2017.2762365.

[14] X. Zhuge, A. G. Yarovoy, T. Savelyev, and L. Ligthart, "Modified kirchhoff migration for UWB MIMO array-based radar imaging," *IEEE Trans. Geosci. Remote Sens.*, vol. 48, no. 6, pp. 2692–2703, Jun. 2010, doi: 10.1109/TGRS.2010.2040747.

[15] H. Liu, Z. Long, F. Han, G. Fang, and Q. H. Liu, "Frequency-domain reverse-time migration of ground penetrating radar based on layered medium Green's functions," *IEEE J. Sel. Topics Appl. Earth Observ. Remote Sens.*, vol. 11, no. 8, pp. 2957–2965, Aug. 2018, doi: 10.1109/JSTARS.2018.2841361.

[16] X. Feng, Y. Yu, C. Liu, and M. Fehler, "Subsurface polarimetric migration imaging for full polarimetric ground-penetrating radar," *Geophys. J. Int.*, vol. 202, no. 2, pp. 1324–1338, 2015, doi: 10.1093/gji/ggv208.

[17] T. Zhu, J. M. Carcione, and M. A. B. Botelho, "Reverse time imaging of ground-penetrating radar and SH-seismic data including the effects of wave loss," *Geophysics*, vol. 81, no. 4, pp. H21–H32, 2016, doi: 10.1190/GEO2015-0397.1.

[18] N. Engheta, C. H. Papas, and C. Elachi, "Radiation patterns of interfacial dipole antennas," *Radio Sci.*, vol. 17, no. 6, pp. 1557–1566, Nov. 1982, doi: 10.1029/RS017i006p01557.

[19] N. Engheta, C. H. Papas, and C. Elachi, "Interface extinction and subsurface peaking of the radiation pattern of a line source," *Appl. Phys. B, Photophysics Laser Chem.*, vol. 26, no. 4, pp. 231–238, Dec. 1981, doi: 10.1007/BF00692543.

[20] D. Comite, A. Galli, I. Catapano, and F. Soldovieri, "The role of the antenna radiation pattern in the performance of a microwave tomographic approach for GPR imaging," *IEEE J. Sel. Topics Appl. Earth Observ. Remote Sens.*, vol. 10, no. 10, pp. 4337–4347, Oct. 2017, doi: 10.1109/JSTARS.2016.2636833.

[21] S. Valle, L. Zanzi, M. Sgheiz, G. Lenzi, and J. Friborg, "Ground penetrating radar antennas: Theoretical and experimental directivity functions," *IEEE Trans. Geosci. Remote Sens.*, vol. 39, no. 4, pp. 749–759, Apr. 2001, doi: 10.1109/36.917886.

[22] V. Pérez-Gracia, D. Di Capua, R. González-Drigo, and L. Pujades, "Laboratory characterization of a GPR antenna for high-resolution testing: Radiation pattern and vertical resolution," *NDT E Int.*, vol. 42, no. 4, pp. 336–344, Jun. 2009, doi: 10.1016/j.ndteint.2008.12.007.

[23] R. Streich, J. van der Kruk, and A. G. Green, "Vector-migration of standard copolarized 3D GPR data," *Geophysics*, vol. 72, no. 5, pp. J65–J75, Sep. 2007, doi: 10.1190/1.2766466.

[24] R. Streich and J. V. van der Kruk, "Accurate imaging of multicomponent GPR data based on exact radiation patterns," *IEEE Trans. Geosci. Remote Sens.*, vol. 45, no. 1, pp. 93–103, Jan. 2007, doi: 10.1109/TGRS.2006.883459.

[25] X. Feng, M. Sato, C. Liu, and Y. Zhang, "Profiling the rough surface by migration," *IEEE Geosci. Remote Sens. Lett.*, vol. 6, no. 2, pp. 258–262, Apr. 2009, doi: 10.1109/LGRS.2008.2011922.

[26] F. Berizzi and G. Corsini, "Autofocusing of inverse synthetic aperture radar images using contrast optimization," *IEEE Trans. Aerosp. Electron. Syst.*, vol. 32, no. 3, pp. 1185–1191, Jul. 1996, doi: 10.1109/7.532282.